Lasers in Manufacturing Conference 2015

Thermal analysis of Laser Transmission Welding of thermoplastics: indicators of weld seam quality

Adhish Majumdar*[a], Benjamin Lecroc[a], Laurent D'Alvise[a]

[a]*Geonx S.A., Rue Santos Dumont 7A, B-6041 Gosselies, Belgium, www.geonx.com*

Abstract

This work presents a thermal analysis of the process of laser transmission welding of thermoplastics using the finite element method. In addition to the heat transfer equations, an original approach was used to calculate phase transformation phenomena such as melting, evaporation or decomposition, and solidification of the polymer. This yields a prediction of the size and shape of the weld seam as well as eventual porosity that may arise due to heating of the plastic beyond its decomposition temperature.

By defining the weld bead quality as a function of its shape, size, and porosity, the results of the simulations with the variation of process parameters can be used to create a mapping between these parameters and the resulting weld quality.

Keywords: joining; laser transmission welding; process simulation;

1. Introduction

Laser transmission welding is a popular method for the joining of plastic parts. Industrial applications of this method are mainly in the automotive sector (Mayboudi et al. 2009). The advantages of the process are the high degree of control that can be exercised and also the low thermal loads involved in welding the parts together. The potential problems in this process are the development of porosity due to gas bubbles formed by the decomposition of the polymer material. The present work presents finite element simulations of the thermal and phase transformation phenomena occurring during the laser transmission welding process. The simulations are set up using Virfac® and its massively parallel finite element solver Morfeo, developed by

* Corresponding author. Tel.: +32 71 960 020; fax: +32 71 960 021.
E-mail address: adhish.majumdar@geonx.com.

GeonX. The simulation results are compared with those presented in literature and analyzed with a view to assess the weld seam quality and its sensitivity to the process parameters.

2. Process description

2.1. Laser transmission welding setup

A schematic diagram of the setup for laser transmission welding setup is shown in Figure 1. The pieces to be welded together are placed in the required configuration, and a clamping system is fixed to hold them in place during welding and more importantly to ensure a good conduction of heat between the parts. Of the two pieces, one is made of a material transparent to the laser wavelength used, while the other is absorbent. The laser radiation incident on the top surface is partly reflected, partly absorbed in the transparent part, and the remaining energy is transmitted down to the absorbent part. The laser radiation is absorbed in the absorbing part to produce heat. This heat is conducted to the transparent part as well. The weld is formed at interface where the temperature exceeds the liquidus temperature of the plastic material.

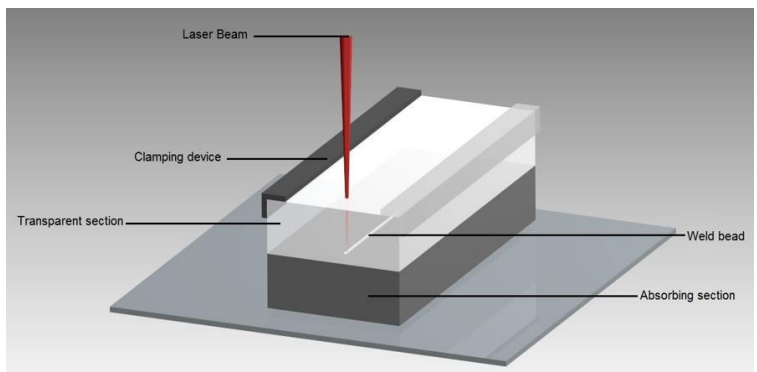

Figure 1 Schematic representation of the laser transmission welding process

Due to the necessity of having one of the parts to be welded being transparent to the laser radiation used and the other absorbing, this welding technique is used to join parts made of dissimilar materials. This limitation is usually overcome by introducing into the lower part particles of a material opaque to the laser radiation such as carbon black (Acherjee et al. 2012a).

2.2. Process parameters

The parameters of the process have significant influence on the quality of the weld formed. The more important parameters are the laser power used, welding speed, and the clamping pressure. Other parameters like the laser spot size, laser beam profile (Gaussian, flat-top, etc.) and the laser wavelength influence the weld quality too, but to a lesser extent. Finally, the material used – especially the characteristics of laser radiation absorption – affects the weld quality.

3. Material

The material of interest in the present work is a polycarbonate. The material properties at different temperatures are taken from literature (Acherjee et al. 2012b) and are represented in Figure 2. The sudden change in the properties at 147 °C represents the glass transition.

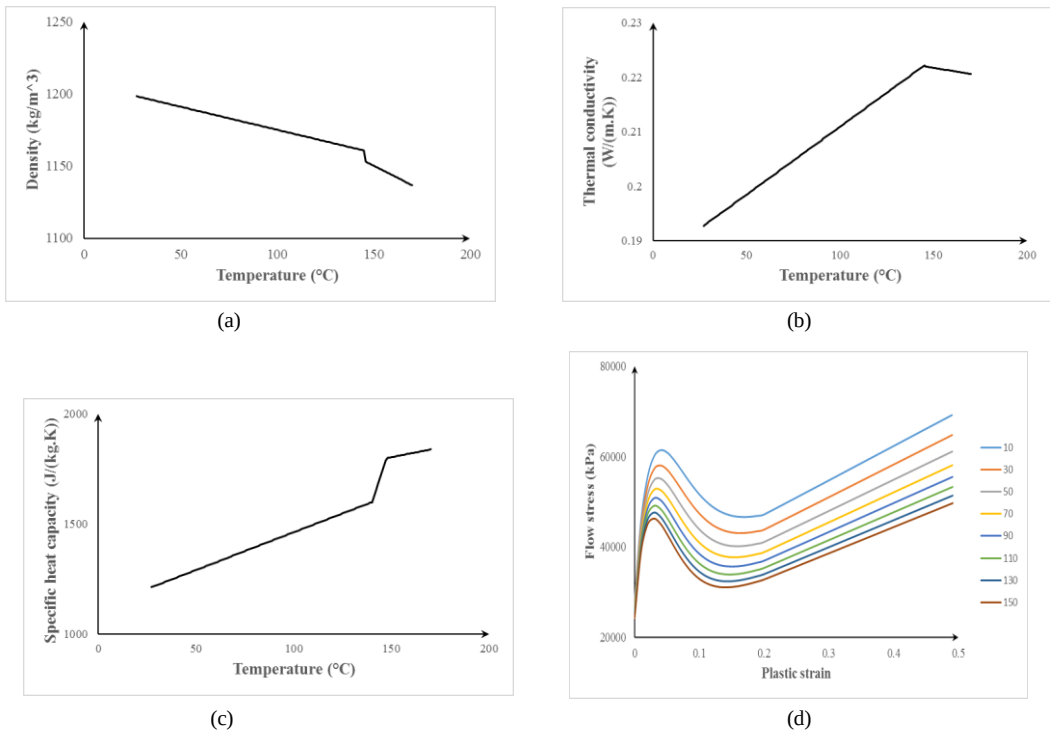

Figure 2 Material properties as functions of temperature: (a) Density, (b) Thermal conductivity, (c) Specific heat capacity (Acherjee et al. 2012b), and (d) Flow stress as a function of plastic strain (Dar et al. 2014)

The mechanical properties of the polycarbonate are represented using stress-strain curves at different temperatures corresponding to a strain rate of 10^{-3} s^{-1} (Dar et al. 2014). The flow stress as a function of plastic strain, for different temperatures is shown in Figure 2(d).

The simulations carried out for this study included the effect of phase transformations. The solid, glassy, liquid, and gas phases were considered. The phases and the transformations between them are represented in Figure 3. The arrows between phases represent the transformations that are defined. Note that the "Gas" phase represents the decomposed polymer, which is why it does not condense back into the liquid state. The "Solid" and "Resolid" phases are identical, but have been defined separately in order to identify the re-solidified zone

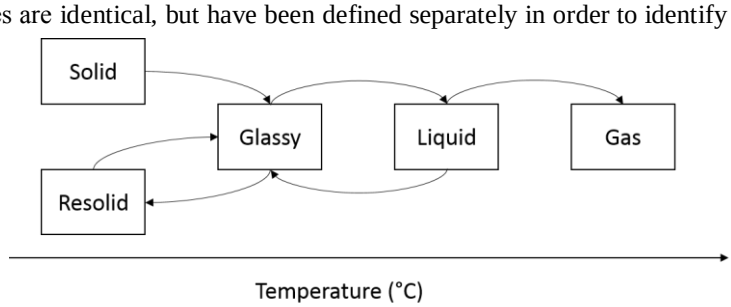

Figure 3 Phase transformations in polycarbonate

which is in fact the weld bead. The solid to glassy transition occurs in the temperature range of 140 – 150 °C, the glassy to liquid transition in 230 – 260 °C, and the polymer decomposes into the gas above 350 °C.

4. Numerical model

4.1. Simulation configuration

The configuration used for the simulations is shown in Figure 4(a). The model considers half of the entire geometry, cut along the plane of symmetry containing the laser beam direction and the laser beam advance direction. Figure 4(b) shows the mesh used in the simulations. A tetrahedral mesh is generated, with 35000 nodes and 175256 elements. The mesh is highly refined in a radius of 0.5 mm around the weld bead, with elements of size 30 µm, and 0.1 mm elsewhere.

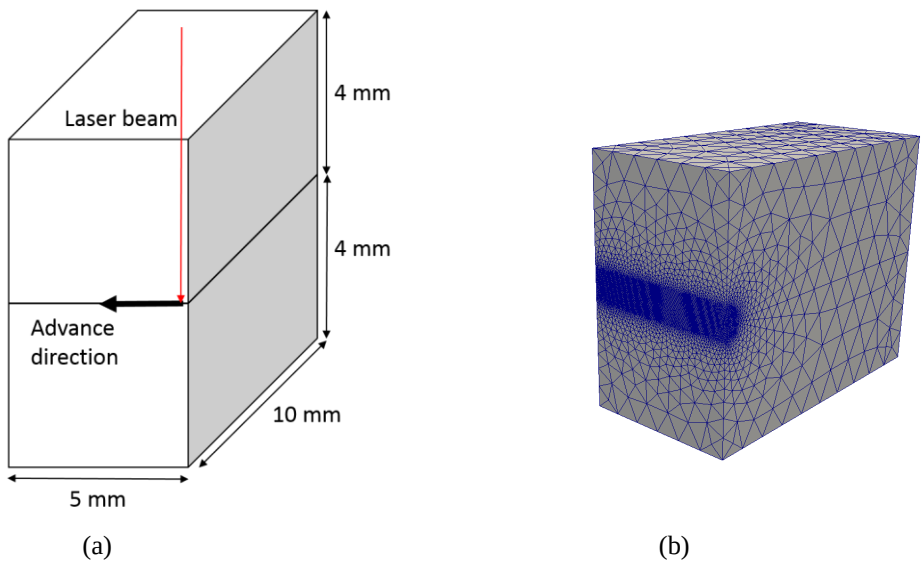

Figure 4 (a) Model of laser transmission welding used in the simulations and (b) the mesh used in the simulations

4.2. Simulation strategy

The simulations are carried out using a staggered transient thermo-mechanical strategy. The thermal problem evaluates the heat source due to absorption of laser radiation, and solves the heat transfer equation to calculate the temperature field. The temperature field is used to determine the phase fractions in each element. Finally the mechanical analysis calculates the displacements, stresses and strains in the welded piece.

The temperature field is calculated using the standard differential equation of heat conduction (equation 1), where T is the temperature, t the time, K the thermal conductivity, ρ the density, C_p the specific heat capacity and Φ the rate of heat generation by absorption of the laser radiation. The heat conduction between the transparent and absorbing sections is considered to be perfect.

$$\frac{\partial T}{\partial t} = \overline{\nabla} \cdot \left(\frac{K}{\rho C_p} \overline{\nabla} T \right) + \dot{\Phi} \tag{1}$$

Balancing the heat generated against the loss of intensity, the rate of heat generation is expressed as the derivative of the laser intensity with respect to the depth in the piece (equation 2).

$$\dot{\Phi} = -\frac{\partial I}{\partial z} \tag{2}$$

Most industrial lasers have a Gaussian intensity profile within the beam and this is the profile used in the simulations. Let us consider a laser of power P, wavelength λ, spot radius R_0 – yielding a Rayleigh length $z_R = (\pi R_0^2/\lambda)$, a focus offset of s, and finally an absorption coefficient α for the material. The laser intensity at a position (x, y, z), in the coordinate system with origin at the point of impingement of the laser and the positive direction of the Z-axis parallel to the laser beam, is evaluated using the Beer-Lambert law giving the expression in equation 3. Deriving this expression with respect to z, and assuming that the Rayleigh length z_R is large compared to the dimensions of the weld piece, we obtain the expression in equation 4 for the rate of heat generation Φ.

$$I(x, y, z) = \frac{2P}{\pi R_0^2 \left[1 + \left(\frac{z - s}{z_R} \right)^2 \right]} e^{-2\left(\frac{x^2 + y^2}{R_0^2} \right)} e^{-\alpha z} \tag{3}$$

$$\dot{\Phi}(x, y, z) = \frac{2\alpha P}{\pi R_0^2 \left[1 + \left(\frac{z - s}{z_R} \right)^2 \right]} e^{-2\left(\frac{x^2 + y^2}{R_0^2} \right)} e^{-\alpha z} \tag{4}$$

In case there is reflection at the surface, the power P should be scaled by the fraction of intensity that is transmitted, thus using $P' = P(1-R)$, where R is the fraction of light reflected. The formulation developed within the solver permits the user to account for absorption in both the upper and lower parts. However, in this study the upper part was assumed to be perfectly transparent to the laser.

Using the temperature fields from the thermal analysis, the phase transformations are evaluated. The phase fraction as a function of temperature between the start and end temperatures of the transformation is expressed as a polynomial function. Finally, the mechanical analysis solves for the nodal displacements and evaluates the stresses within the piece.

The plane of symmetry is blocked in the direction normal to it, and is considered to be adiabatic representing the symmetry condition. The top and bottom faces are blocked in accordance with a clamped condition. Ideally, convection and radiation conditions should be applied to all the external surfaces. However, it has been observed that these surfaces remain at temperatures close to the ambient temperature due to the extremely low thermal diffusivity of polycarbonate. Therefore the thermal boundary conditions of radiation and convection are not applied.

The simulations were carried out with the parameters provided in Table 1. Two simulations are presented in this article, with all the process parameters held constant except the laser advance velocity. These parameters correspond to those used in experiments presented in (Russek et al. 2004), and the simulation results will be compared against them.

Table 1. Process parameters considered in the simulation

Process parameter	Symbol	Value	Unit
Coefficient of absorption (upper block)	α_{upper}	0.0	mm^{-1}
Coefficient of absorption (lower block)	α_{lower}	15.873	mm^{-1}
Laser power	P	10.0	W
Spot size	R_0	424.26	µm
Reflectance (upper surface)	R_{upper}	0.07	-
Reflectance (interface)	$R_{interface}$	0.07	-
Laser advance speed	V	125, 166.67	mm s^{-1}

5. Results and discussion

This section presents the results of the simulation in terms of the shape and size of the weld bead, and the presence or absence of defects such as gas bubbles in the weld bead.

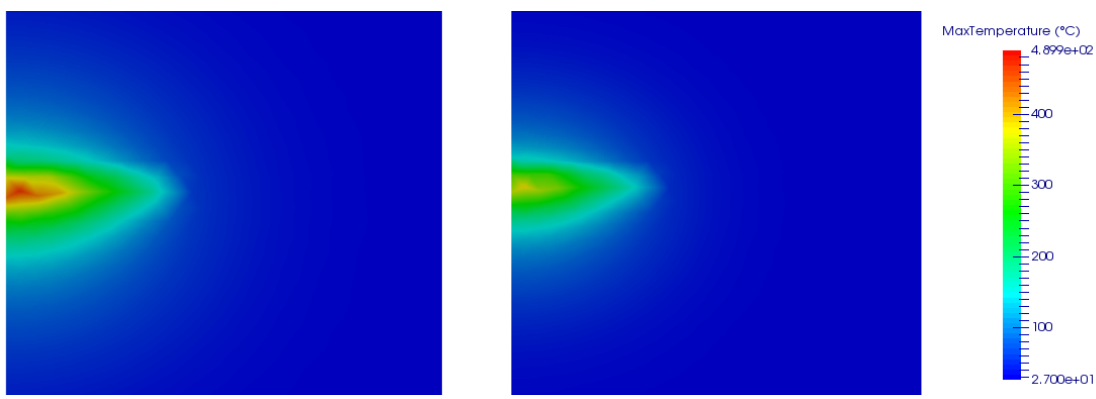

(a) (b)

Figure 5 Maximum temperature in the weld, looking along the advance direction of the laser for (a) v=125 mm/s, (b) v = 166.67 mm/s

Figure 5 shows the maximum temperature attained in the weld zone (in the plane containing the laser beam direction and the weld trajectory). For the lower velocity case (Figure 5 (a)), the amount of energy deposited per unit length (the line energy) is higher. Therefore the maximum temperature attained is higher for this case compared to the higher velocity case (Figure 5(b)). The heated zone is also larger.

The evolution of the volume fractions of the phases during the simulation is also calculated. The parts of the geometry where welding takes place, the material passes from 100% solid, to glassy, liquid, and

eventually gas during heating as the laser passes over the point. Subsequently, the liquid cools down to glassy and then resolid, while the gas remains unchanged. By filtering on the presence of the phase “Resolid” with a minimum threshold of 1% (meaning at least 1% of material is molten and resolidified), the form of the weld bead is obtained. This is displayed in Figure 6. This figure also shows the volume fraction of the gas phase inside the weld bead. For the simulation with lower velocity, we observe the presence of approximately 20% of the gas phase near the center of the weld bead. The weld is thus porous and may be considered to be of poor quality. For the higher velocity case, no gas phase is observed, and thus the weld bead is free of defects.

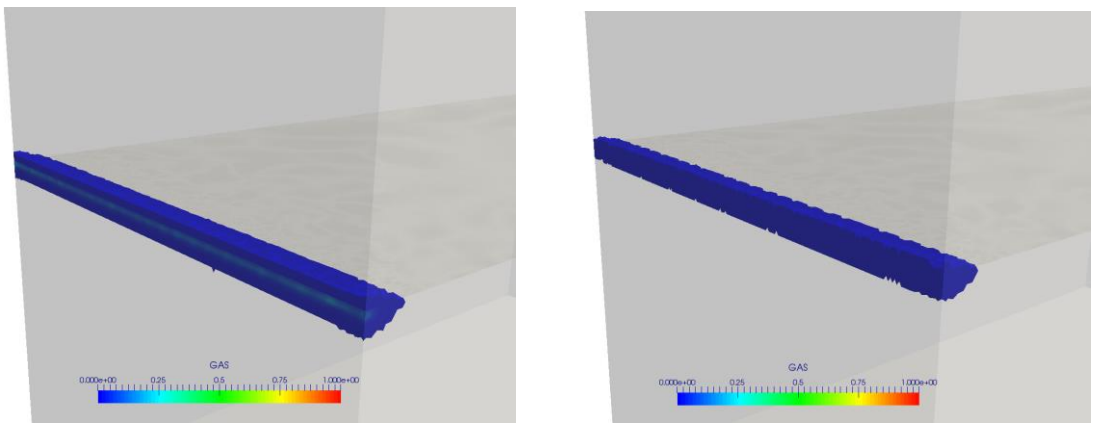

(a) (b)

Figure 6 Form of the weld bead, showing percentage of gas in the weld for the process with (a) v = 125 mm/s, (b) v = 166.67 mm/s

The dimensions of the weld bead were measured using the definitions shown in Figure 7. Note that the effective width of the weld is smaller than its maximum width which lies within the absorbing part. The final measured dimensions are listed in Table 2, alongside corresponding measurements by (Russek et al. 2004). The predictions for the weld width are in very good agreement with the experimental results. The precision is slightly lower for the depth values, but it remains close to those observed in the experiments. This is most likely due to the assumption of perfect transparence of the upper part, which is not strictly true in practice.

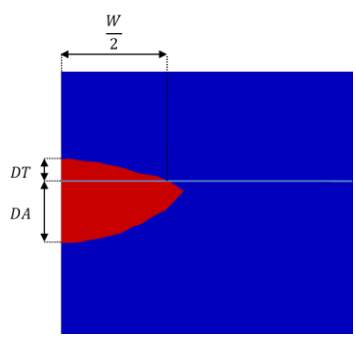

Figure 7 Definition of the weld bead dimensions

Table 2. Weld bead dimensions from the simulations compared with those from experiments (Russek et al. 2004)

Welding speed (mm s^{-1})	Weld bead dimension	Simulations (µm)	Experiments (µm)
125	W/2	626	515
125	DT	62	32
125	DA	169	131
166.67	W/2	558	549
166.67	DT	34	25
166.67	DA	136	116

6. Conclusions

This study presents finite element simulations of the laser transmission welding of polycarbonate using Virfac® and its FE solver Morfeo. The heat generation within the weld is evaluated using the Beer-Lambert law for the absorption of laser radiation. The phase transformation calculations evaluate the liquefaction, resolidification, and eventual decomposition of the material to provide the final form of the weld bead and porosity that may develop within it. The weld bead dimensions obtained in the simulations were compared with those reported in literature and a very good agreement was observed.

Acknowledgements

The authors would like to thank the ERA-Net (MANUNET) project no. 1317976 "WELDABLE" for financing the research and development leading to the simulations presented in this article. The authors also appreciate the support of the project coordinator Dr. Cédric Volcke.

References

Acherjee, B. et al., 2012a. Effect of carbon black on temperature field and weld profile during laser transmission welding of polymers: A FEM study. *Optics & Laser Technology*, 44(3), pp.514–521. Available at: http://linkinghub.elsevier.com/retrieve/pii/S0030399211002362 [Accessed August 18, 2014].

Acherjee, B. et al., 2012b. Modeling of laser transmission contour welding process using FEA and DoE. *Optics and Laser Technology*, 44(5), pp.1281–1289. Available at: http://linkinghub.elsevier.com/retrieve/pii/S0030399211004518 [Accessed August 18, 2014].

Dar, U.A. et al., 2014. Thermal and strain rate sensitive compressive behavior of polycarbonate polymer - experimental and constitutive analysis. *Journal of Polymer Research*, 21(8). Available at: http://link.springer.com/10.1007/s10965-014-0519-z.

Mayboudi, L.S. et al., 2009. Infrared observations and finite element modeling of a laser transmission welding process. *Journal of Laser Applications*, 21(August), pp.111–118.

Russek, U.A. et al., 2004. Laser beam welding of thermoplastics parameter influence on weld seam quality - experiments and modeling. In *23rd International Congress on Applications of Lasers and Electro Optics*.